Desalination and Water Treatment
www.deswater.com

doi: 10.5004/dwt.2020.26011

198 (2020) 364–375
September

Synthesis, characterization, and photocatalytic activity of a novel Bi_2O_3/Ag_3VO_4 heterojunction photocatalyst

Chung-Hsin Wu[a,*], Chao-Yin Kuo[b], Cheng-Di Dong[c], Chiu-Wen Chen[c], Yi-Li Lin[d], Yu-Sheng Kuan[a]

[a]*Department of Chemical and Materials Engineering, National Kaohsiung University of Science and Technology, 415 Chien Kung Road, Kaohsiung, Taiwan, Tel. +886-7-3814526; Fax: +886-7-3830674; email: wuch@nkust.edu.tw (C.-H. Wu), Tel. +886-7-3814526; email: daniel_kuan@hotmail.com (Yu-Sheng Kuan)*
[b]*Department of Safety, Health and Environmental Engineering, National Yunlin University of Science and Technology, Yunlin, Taiwan, Tel. +886-5-5347311; email: kuocyr@ms35.hinet.net (C.-Y. Kuo)*
[c]*Department of Marine Environmental Engineering, National Kaohsiung University of Science and Technology, Kaohsiung, Taiwan, Tel. +886-7-3617141; email: cddong@nkust.edu.tw (C.-D. Dong), Tel. +886-7-3617141; email: cwchen@nkust.edu.tw (C.-W. Chen)*
[d]*Department of Safety, Health and Environmental Engineering, National Kaohsiung University of Science and Technology, Kaohsiung, Taiwan, Tel. +886-7-6011000; email: yililin@nkust.edu.tw (Y.-L. Lin)*

Received 28 January 2020; Accepted 20 April 2020

ABSTRACT

In this investigation, the single-step hydrothermal method is used to synthesize novel Bi_2O_3/Ag_3VO_4 heterojunction photocatalysts (BAVs). BAVs were generated under different Bi_2O_3/Ag_3VO_4 molar ratios and their photocatalytic activity was evaluated by using them to degrade C.I. Reactive Red 2 (RR2) under ultraviolet (UV), visible-light (Vis.) or solar irradiation. The morphological, structural, and spectroscopic properties of the prepared samples were determined using X-ray diffraction (XRD), scanning electron microscopy, transmission electron microscopy (TEM), specific surface area analysis, UV-Vis. diffuse reflectance spectral analysis, photoluminescence spectral analysis, and X-ray photoelectron spectroscopy (XPS). Surface analyses by XRD, TEM, and XPS revealed that the interaction between Ag_3VO_4 and Bi_2O_3 involved chemical bonding rather than simple physical mixing. The BET surface areas of Ag_3VO_4, Bi_2O_3, and 1BAV were 0.18, 0.94, and 1.11 m^2/g, respectively. The photodegradation of RR2 was consistent with the pseudo-first-order model and the optimal Bi_2O_3/Ag_3VO_4 molar ratio was unity (1BAV). The rate constants of RR2 photodegradation by Ag_3VO_4, Bi_2O_3, and 1BAV under Vis. irradiation were 0.048, 1.50, and 3.16 h^{-1}, respectively. The enhanced photocatalytic performance of 1BAV was attributed to the reduced recombination probability of the photo-generated electrons and holes. Coupling Ag_3VO_4 with Bi_2O_3 could reduce the leaching of Ag from Ag_3VO_4 during photodegradation. The experimental results indicate that photo-generated holes and superoxide anion radicals were the predominant active species in 1BAV.

Keywords: Ag_3VO_4; Bi_2O_3; Heterojunction; Hydrothermal; Photocatalysis

* Corresponding author.

1. Introduction

Advanced oxidation processes are attractive for degrading environmental contamination because they can completely decompose pollutants into carbon dioxide and water under ambient conditions. Semiconductor photocatalysis is a cost-effective and environmentally friendly method for solar energy utilization and environmental remediation. The development of new photocatalysts that are effective under visible-light (Vis.) is always favorable because the sun emits plenty of Vis. Silver vanadate (Ag_3VO_4), which was first synthesized by Konta et al. [1], exhibited photocatalytic activity in the evolution of O_2 from H_2O under Vis. irradiation and has therefore attracted considerable attention. However, Ag_3VO_4 suffers from serious photo-corrosion and recombination of photo-generated electrons and holes during photocatalysis. Generally, the construction of heterojunctions is an efficient and simple method for developing highly efficient photocatalysts [2,3]. This method yields a hybrid photocatalyst that benefits from such synergistic effects as high light-harvesting ability, efficient photo-generated electron-hole separation, and high photo-stability, and therefore exhibited photo-activity that is remarkably higher than single-photocatalyst [4].

Other catalysts are coupled with Ag_3VO_4 to promote the separation of photo-generated electron-hole pairs, improving its photo-activity. Ag_3VO_4 can be combined with such semiconductors as g-C_3N_4 [5–7], BiOCl [8], TiO_2 [9], La_2O_3 [10], $CoTiO_3$ [11], Bi_2WO_6 [12,13], $CaFe_2O_4$ [14], Co_3O_4 [15], $ZnFe_2O_4$ [16], BiOI [17], NiO [18,19], $Ag_2VO_2PO_4$ [20], $BiOIO_3$ [21], and BiOBr [22] to form heterojunctions with improved photocatalytic performance as a result of the reduction of the recombination probability of the photo-generated electrons and holes.

Wu et al. [6] used the deposition–precipitation method to synthesize the heterojunction g-C_3N_4/Ag_3VO_4, which exhibited high efficiency in the degradation of rhodamine B (RhB) under Vis. irradiation. The excellent photocatalytic performance of g-C_3N_4/Ag_3VO_4 is attributable to the matched band structures of Ag_3VO_4 and g-C_3N_4. The 40 wt.% g-C_3N_4/Ag_3VO_4 photocatalyst exhibited the highest basic fuchsin removal rate constant of 0.92 h^{-1}, which was 11.5 and 6.6 times higher than those of pure g-C_3N_4 and Ag_3VO_4, respectively [5]. Zhu et al. [7] found a reaction rate constant of 5 wt.% g-C_3N_4/Ag_3VO_4 for photocatalyzed RhB degradation, which was 8.25 times that of pure Ag_3VO_4. 5 wt.% g-C_3N_4/Ag_3VO_4 composite has remarkably higher current responses than pure Ag_3VO_4 or g-C_3N_4, suggesting more efficient separation and the longer lifetime of photo-excited electron-hole pairs. Xu et al. [10] synthesized La_2O_3/Ag_3VO_4 by impregnation and found a rate of photocatalytic degradation of RhB by 3 wt.% La_2O_3/Ag_3VO_4 that was 2.8 times that by pure Ag_3VO_4. The high photocatalytic activity of Ag_3VO_4/TiO_2 can be attributed to its strong absorption in the Vis. region and its excellent charge separation characteristics [9]. Ag_3VO_4/Bi_2WO_6 heterojunctions exhibited 6.7 or 1.7 times greater photo-activity than pure Bi_2WO_6 or Ag_3VO_4. Introducing Ag_3VO_4 inhibits the recombination of photo-generated electron-hole pairs in Bi_2WO_6, increasing photocatalytic activity and providing good stability [12]. Co_3O_4/Ag_3VO_4 exhibited high photocatalytic efficiency in the degradation of RhB under Vis. irradiation, and its highest photocatalytic activity has been obtained using a sample that was calcined at 653 K with 1.0 wt.% Co, which was incorporated by the impregnation method [15]. The rate of degradation of RhB by $ZnFe_2O_4$/Ag_3VO_4 samples has a maximum value of 4.82 h^{-1}, which is 4.6 and 10.8 times the rates achieved using pure Ag_3VO_4 and N-doped TiO_2, respectively [16]. Wangkawong et al. [11] has suggested that the formation of a heterojunction between $CoTiO_3$ and Ag_3VO_4 increases the Vis.-harvesting ability of the composite and provides efficient photo-generated electron-hole separation, increasing the number of active species that are generated in the hybrid system consequently providing excellent photocatalytic activity. The construction of a heterojunction between $Ag_2VO_2PO_4$ and Ag_3VO_4 can accelerate the separation of photo-induced electron-hole pairs and is probably responsible for the enhanced photo-activity [20].

Although many Ag_3VO_4-based/contained photocatalysts have been developed, the development of novel Ag_3VO_4-based/contained photocatalysts is still pursued to enrich this family of photocatalysts [21]. To the best of our knowledge, the improvement of the photocatalytic performance of Ag_3VO_4 by Bi_2O_3 coupling has not been reported upon. In this study, the single-step hydrothermal method is used to synthesize Bi_2O_3/Ag_3VO_4 heterojunction photocatalysts (BAVs) with various Bi_2O_3/Ag_3VO_4 molar ratios, whose photocatalytic activities in the degradation of C.I. Reactive Red 2 (RR2) under ultraviolent (UV) or Vis. irradiation are compared. The goals of this study are (i) to synthesize BAVs with different Bi_2O_3/Ag_3VO_4 molar ratios; (ii) to measure the surface characteristics and compare the photocatalytic activities of the prepared BAVs, and (iii) to determine the reusability and the active reaction species of BAVs at the optimal Bi_2O_3/Ag_3VO_4 molar ratio.

2. Materials and methods

2.1. Materials

Silver nitrate ($AgNO_3$) and RR2 ($C_{19}H_{10}Cl_2N_6Na_2O_7S_2$) were obtained from Sigma-Aldrich (USA). Bismuth (III) nitrate ($Bi(NO_3)_3{\cdot}5H_2O$), sodium hydroxide (NaOH), nitric acid (HNO_3), sodium nitrite ($NaNO_2$), disodium ethylenediamine tetraacetate (EDTA-2Na, $C_{10}H_{14}N_2O_8Na_2{\cdot}2H_2O$) and potassium chromate (K_2CrO_4) were all purchased from Katayama (Japan). Sodium orthovanadate (Na_3VO_4) and isopropanol (IPA) were obtained from Alaf–Aesar (USA) and J.T. Baker (USA), respectively. All chemicals were of analytical reagent grade and used without further purification or treatment. Deionized (D.I.) water was used throughout this study.

2.2. Synthesis of Ag_3VO_4, Bi_2O_3, and BAVs

The BAVs were prepared via the single-step hydrothermal process, the details of which are as follows. 3.0567 g of $AgNO_3$ and 1.226 g of Na_3VO_4 were dissolved in 60 mL D.I. water to yield solutions A and B, respectively. The desired amount of $Bi(NO_3)_3{\cdot}5H_2O$ (0.7425, 1.485, 2.2275, and 2.97 g) was added to 20 mL D.I. water to form solution C. The obtained mixture of solutions A, B, and C were adjusted

to pH 13 by adding 10 M NaOH or HNO_3 and stirring (600 rpm) for 30 min. Then the above mixture was sealed in a 200 mL Teflon-lined stainless autoclave and maintained at 393 K for 6 h. When the autoclave was cooled naturally to room temperature, the products were harvested by centrifugation, washed several times using D.I. water and alcohol, and dried in an oven at 333 K for 12 h to yield BAVs. Four Bi_2O_3/Ag_3VO_4 molar ratios (0.25, 0.5, 0.75, and 1.0) were used in the syntheses, yielding 0.25BAV, 0.5BAV, 0.75BAV, and 1BAV. Ag_3VO_4 was prepared using a Ag/V molar ratio of three without the addition of $Bi(NO_3)_3{\cdot}5H_2O$. When no $AgNO_3$ or Na_3VO_4 was added, the obtained powder was Bi_2O_3. The experimental conditions and procedures for synthesizing Bi_2O_3 and Ag_3VO_4 were the same as those for generating BAVs.

2.3. Surface analyses of photocatalysts

The X-ray diffraction (XRD) patterns of the photocatalysts were obtained using an X-ray diffractometer (Bruker D8 SSS, Germany) with Cu radiation (λ = 0.15418 nm) in the 2q range from 20° to 80°. The morphology of the photocatalysts was observed using a scanning electron microscopy (SEM, JEOL 6330 TF, Japan) and a transmission electron microscopy (TEM, JEOL 3010, Japan). UV-Vis. diffuse reflectance spectra (DRS) of the photocatalysts were obtained on a UV-Vis spectrophotometer (JAS.CO-V670, Japan). The specific surface areas of the prepared powders were measured by nitrogen adsorption/desorption using the Brunauer–Emmett–Teller (BET) method (Micromeritics ASAP 2020, USA). Photoluminescence (PL) spectra were recorded using a spectrophotometer (Hitachi F-4500, Japan) with an excitation wavelength of 350 nm at room temperature. X-ray photoelectron spectroscopy (XPS) measurements were made at room temperature using a PHI 5000 Versal Probe X-ray photoelectron spectrometer (USA). The binding energies were calibrated against C_{1s} at 284.6 eV. The concentration of Ag that leached from photocatalysts during photodegradation was measured by inductively coupled plasma-optical emission spectrometry (Perkin Elmer Optima 5300DV, USA).

2.4. Photodegradation experiments

The photocatalyst dosage, RR2 concentration, pH and temperature in all of the experiments were 0.5 g/L, pH 3, 20 mg/L, and 298 K, respectively. Photocatalysis experiments were conducted in a 3 L glass reactor. The light source was a 400 W Xe lamp (200 nm < wavelength < 700 nm, UniVex BT-580, Taiwan) with a light intensity of 30.3 mW/cm^2. A quartz appliance that was filled with 2 M $NaNO_2$ solution was placed on the top of the reactor to absorb the UV and to provide only Vis. [23]. The temperature of the reactor was maintained at 298 K using circulating water. The solution was mechanically stirred and continuously aerated by a pump to provide air and ensure complete mixing. To identify the main active species in the photocatalytic system, EDTA-2Na, IPA, and $K_2Cr_2O_7$ as active scavengers of photo-generated holes (h^+) [24–26], hydroxyl radical ($^{\bullet}OH$) [26,27] and superoxide anion radical ($^{\bullet}O^{2-}$) [28], respectively, were separately added during the photocatalytic reaction. In the photocatalytic experiments, the concentration of scavengers added equaled that of photocatalyst added. The stability and reusability of 1BAV were evaluated under the same conditions in the photocatalytic experiments. At the end of each cycle, the recovered 1BAV was centrifuged and dried at 333 K for 24 h. The resulting powder was then used in the next cycle. Solar irradiation experiments were performed on the top floor of the building of the Department of Chemical and Materials Engineering (22.648907 N, 120.327666 E). The reactions were conducted between 12:00 and 13:00. Samples were taken from the reactor at regular intervals and the photocatalyst was removed for spectrophotometric analysis (Hitachi U5100, Japan). The absorbance of the supernatant was analyzed at the 538 nm peak to determine the concentration of RR2 at different times. The photocatalytic experiments were performed in triplicate and mean values were reported.

3. Results and discussion

3.1. Surface characteristics of Ag_3VO_4, Bi_2O_3, and BAVs

The crystalline phases of the prepared Ag_3VO_4, Bi_2O_3, and BAVs were studied by XRD analysis. Fig. 1 displays the XRD results for the Ag_3VO_4, Bi_2O_3, and BAVs. The XRD patterns of all photocatalysts exhibited high diffraction peak intensities, indicating that the catalysts were well crystallized. For pure Ag_3VO_4, the 2q values of 30.8° and 32.3° correspond to the lattice planes of (–1 2 1) and (1 2 1), respectively, and for pure Bi_2O_3, the 2q value of 27.9° corresponds to the lattice plane of (–1 2 1). The observed patterns indicate that the prepared Ag_3VO_4 and Bi_2O_3 both had monoclinic structures, corresponding to JCPDs Nos. 43-0542 and 27-0053, respectively. BAVs yielded peaks that corresponded to a mixture of monoclinic Ag_3VO_4 and Bi_2O_3, and the intensities of the Bi_2O_3 peaks increased gradually with the Bi_2O_3 content. No other crystalline phase was detected, and no sharp diffraction peak was observed, suggesting that the composite samples were very pure.

The microstructures and morphologies of the photocatalyst were investigated by SEM and TEM, as presented in Figs. 2 and 3, respectively. The morphologies of Ag_3VO_4 (Fig. 2a) and Bi_2O_3 (Fig. 2b) were those of pebble-like micelles and cylindrical micelles, respectively. The 0.75BAV and 1BAV samples comprised highly agglomerated particles with some rod-shaped assembles and rough surfaces (Figs. 2c and d). All photocatalysts had sizes of several micrometers. Pure Ag_3VO_4 (Fig. 3a) and Bi_2O_3 (Fig. 3b) were obtained as irregular particles and sheets, respectively. TEM clearly revealed the close interfacial connections between Ag_3VO_4 and Bi_2O_3 in the 1BAV (Fig. 3c), which consisted of sheets (Bi_2O_3) and particles (Ag_3VO_4), and the particles attached tightly to the surfaces of the sheets (Fig. 3c), indicating that the Bi_2O_3/Ag_3VO_4 heterojunction had formed.

Table 1 lists the specific surface areas of all of the samples. The BET surface areas of Ag_3VO_4, Bi_2O_3, 0.25BAV, 0.5BAV, 0.75BAV, and 1BAV were 0.18, 0.94, 0.65, 1.07, 0.92, and 1.11 m^2/g, respectively. The BET surface areas of BAVs exceeded that of Ag_3VO_4 because they had rougher surfaces, which provided more photocatalytic active sites, favoring

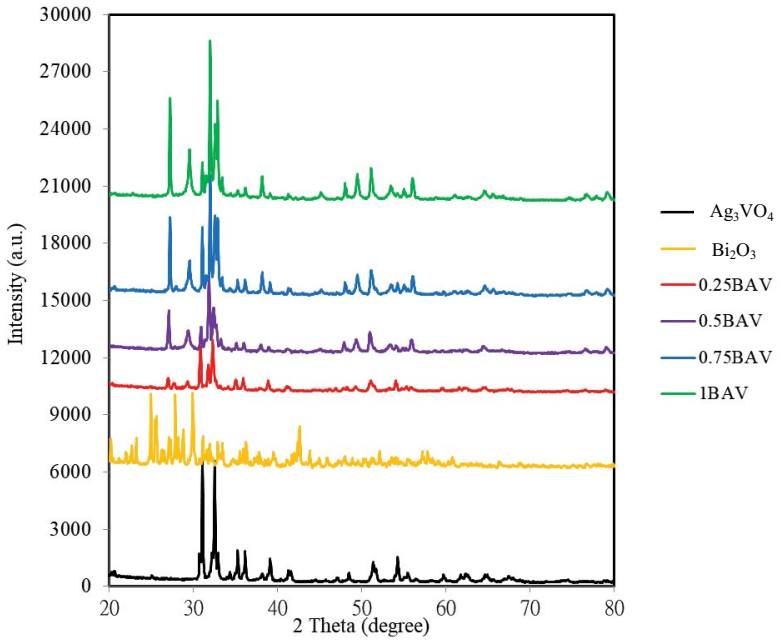

Fig. 1. XRD patterns of Ag_3VO_4, Bi_2O_3, and BAVs.

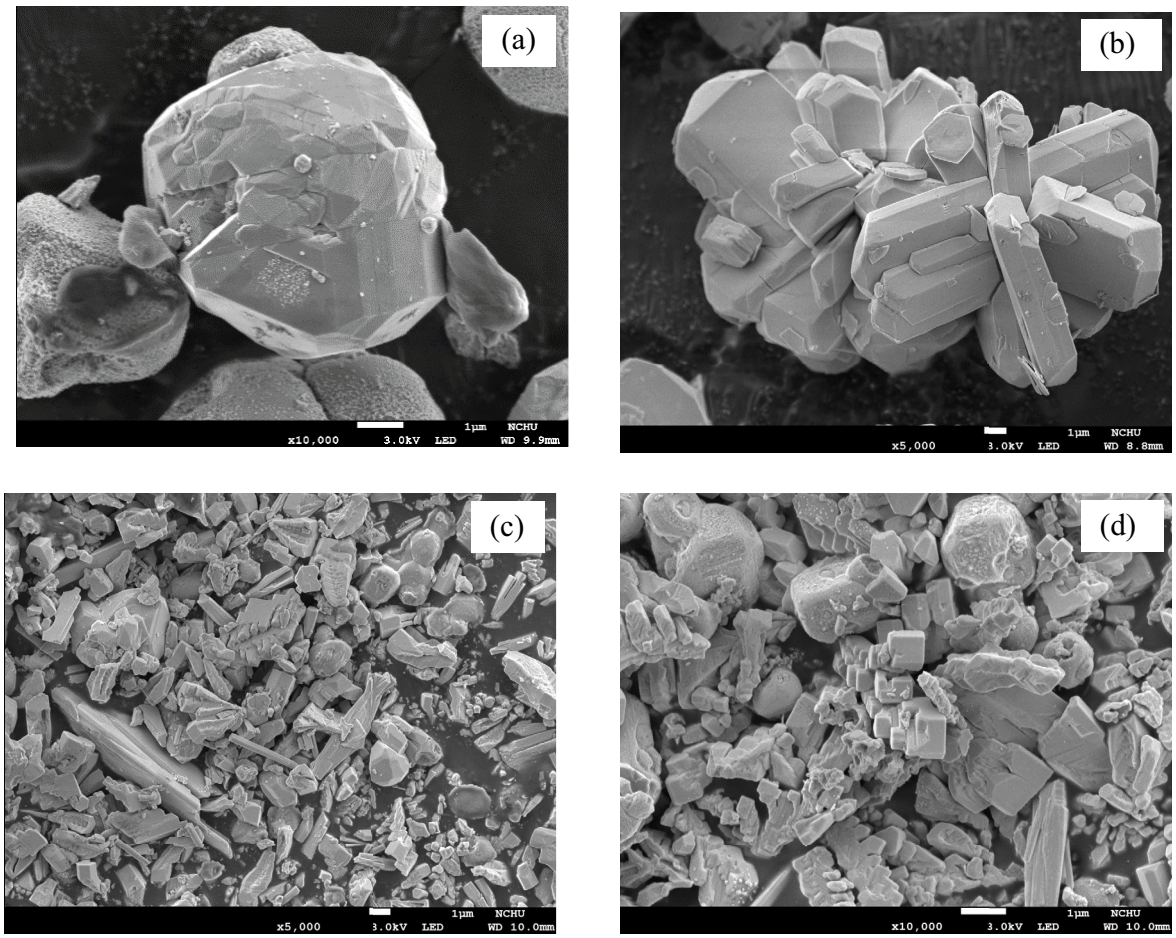

Fig. 2. SEM image of photocatalyst (a) Ag_3VO_4, (b) Bi_2O_3, (c) 0.75BAV, and (d) 1BAV.

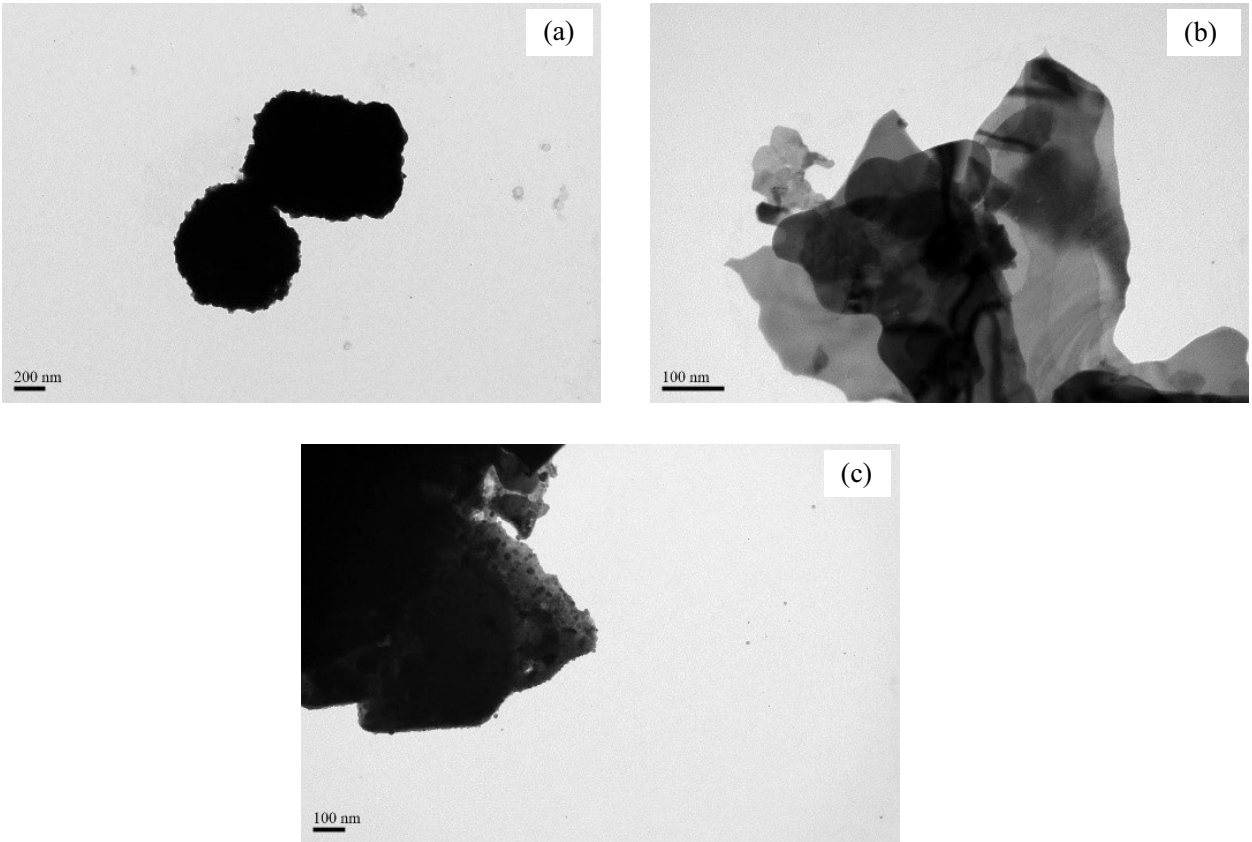

Fig. 3. TEM image of photocatalyst (a) Ag_3VO_4, (b) Bi_2O_3, and (c) 1BAV.

Table 1
Surface characteristics of prepared photocatalysts

Photoatalysts	BET surface area (m^2/g)	Band gap (eV)	UV		Visible-light	
			k (h^{-1})	R^2	k (h^{-1})	R^2
Ag_3VO_4	0.18	1.8	0.618 (0.300)*	0.950 (0.822)*	0.048	0.897
Bi_2O_3	0.94	3.7	0.468	0.912	0.150	0.997
0.25BAV	0.65	2.6	0.540	0.931	0.108	0.998
0.5BAV	1.07	2.3	4.13	0.970	0.168	0.930
0.75BAV	0.92	2.7	5.59 (4.79)*	0.992 (0.960)*	1.65	0.981
1BAV	1.11	2.4	4.97 (14.7)*	0.965 (0.913)*	3.16	0.940

()*: solar.

photocatalysis. Their BET surface areas are of the same magnitude, and very low.

The light absorption properties of Ag_3VO_4, Bi_2O_3, and BAVs were analyzed using UV-Vis absorption spectroscopy. The DRS of the photocatalysts were used to determine the band gap (data not shown here). All photocatalysts except Bi_2O_3 exhibited intense absorption in the Vis. region. The band gaps of the photocatalysts were calculated from the DRS using the formula, band gap (eV) = 1,240/λ (nm), where λ is the absorption edge of the photocatalyst. The band gaps of Ag_3VO_4, Bi_2O_3, 0.25BAV, 0.5BAV, 0.75BAV, and 1BAV were 1.8, 3.7, 2.6, 2.3, 2.7, and 2.4 eV, respectively (Table 1).

Fast photo-generated electron-hole pair separation is associated with high photocurrent generation and highly efficient photocatalytic activity. The PL technique was used to compare the rates of recombination of photo-generated electron-hole pairs in the samples. Generally, higher fluorescence intensity corresponds to a higher rate of recombination of photo-generated carriers and a lower photocatalytic activity [29–31]. Fig. 4 plots the PL spectra of Ag_3VO_4, Bi_2O_3, and BAVs. The PL intensities followed the order Bi_2O_3 > Ag_3VO_4 = 0.25BAV > 1BAV ≧ 0.75BAV > 0.5BAV. Coupling Ag_3VO_4 with Bi_2O_3 accelerated the interfacial charge transfer to the electron acceptor and increased the effectiveness

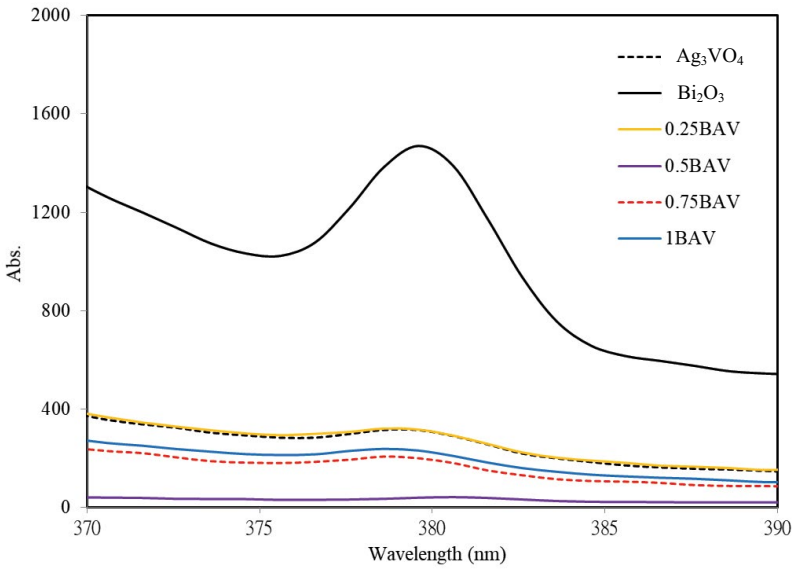

Fig. 4. PL spectra of Ag_3VO_4, Bi_2O_3, and BAVs.

of separation of the photo-generated electron-hole pairs, improving photocatalytic activity.

XPS analysis was performed to determine the elemental composition and chemical state of 1BAV. In Fig. 5a, two peaks are observed at 367.5 and 373.6 eV, corresponding to the binding energy of Ag and to $Ag_{3d5/2}$ and $Ag_{3d3/2}$, respectively, which are characteristic of Ag^+ [9,15,21,32]. In Fig. 5b, binding energies of 515.6 and 523.2 eV are observed, corresponding to $V_{2p3/2}$ and $V_{2p5/2}$ in 1BAV, which are characteristic of the V^{5+} oxidation state [9,21,33,34]. The peaks of $Bi_{4f7/2}$ and $Bi_{4f5/2}$ at 158.2 and 163.7 eV, respectively (Fig. 5c) are characteristic of Bi^{3+} ions [17]. Fig. 5d displays the asymmetrical O_{1s} signal and the peaks at 529.1, 529.7, 530.6, and 531.6 eV, which are attributed to the Ag–O [17], Bi–O [17,35], V–O, and –OH [10,36,37] bonds, respectively. The peaks at 530–531.4 eV are attributed to the lattice oxygen in the heterogeneous multi-phase photocatalysts [38]. Therefore, the peak at 530.6 eV was suggested herein to be associated with the V–O bond. Surface analyses indicate that the interaction between Ag_3VO_4 and Bi_2O_3 is one of chemical bonding rather than simple physical mixing.

3.2. Photocatalytic activity of Ag_3VO_4, Bi_2O_3, and BAVs

Experiments on the adsorption of RR2 on Ag_3VO_4, Bi_2O_3, and BAVs in the dark were carried out. After 180 min of adsorption, the RR2 adsorption efficiencies of Ag_3VO_4, Bi_2O_3, 0.25BAV, 0.5BAV, 0.75BAV, and 1BAV were 8%, 26%, 5%, 20%, 5%, and 6%, respectively. The results reveal low adsorption on the surfaces of the photocatalysts except for Bi_2O_3 and 0.5BAV (Fig. 6a). Generally, a higher surface area of the adsorbent results in a higher adsorption capacity. However, the adsorption of RR2 did not vary with surface area in that way and RR2 adsorption was not apparently correlated with the surface area of BAVs herein.

The photocatalytic activities of Ag_3VO_4, Bi_2O_3 and BAVs in the photodegradation of RR2 under UV or Vis. irradiation were examined. Figs. 6b and 6c show the photocatalytic activities of all photocatalysts under Vis. and UV irradiation. After 180 min of reaction, the percentage of the photocatalysis of RR2 under Vis. irradiation by Ag_3VO_4, Bi_2O_3, 0.25BAV, 0.5BAV, 0.75BAV, and 1BAV were 23%, 39%, 37%, 46%, 94%, and 96%, respectively (Fig. 6b). After 60 min of reaction, the percentage of the photocatalysis of RR2 under UV irradiation by Ag_3VO_4, Bi_2O_3, 0.25BAV, 0.5BAV, 0.75BAV, and 1BAV were 53%, 44%, 60%, 91%, 98%, and 95%, respectively (Fig. 6c). The photocatalytic efficiencies of pure Ag_3VO_4 and Bi_2O_3 were relatively low. 0.75BAV and 1BAV exhibited better photocatalytic performance than pure Ag_3VO_4 and Bi_2O_3 (Figs. 6b and c). Bi_2O_3 exhibited lower photo-activity than BAVs under UV irradiation, possibly because of the significantly higher rate of recombination of photo-generated electrons and holes in Bi_2O_3 than in BAVs, as supported by the PL study. Fig. 7 plots the effects of light source on RR2 photodegradation in the Ag_3VO_4, 0.75BAV and 1BAV systems. After 60 min of reaction, the percentages of the RR2 that Ag_3VO_4, 0.75BAV, and 1BAV photocatalyzed by solar irradiation, were 13%, 94%, and 97%, respectively. Both 0.75BAV and 1BAV exhibited high photocatalytic activity under Vis., UV, and solar irradiation.

The photocatalytic degradation of RR2 closely fitted the following pseudo-first-order equation (Eq. (1)) [6,12,19,21,39].

$$\ln\left(\frac{C_0}{C}\right) = k_t \tag{1}$$

where C_0 and C denote the initial and residual concentrations of RR2 solution; t is the reaction time (h), and k is the reaction rate constant (h^{-1}). The k values of Vis. photocatalysis followed the order 1BAV > 0.75BAV > 0.5BAV > Bi_2O_3 > 0.25BAV > Ag_3VO_4; moreover, and those of UV photocatalysis followed the order 0.75BAV > 1BAV > 0.5BAV > Ag_3VO_4 >>

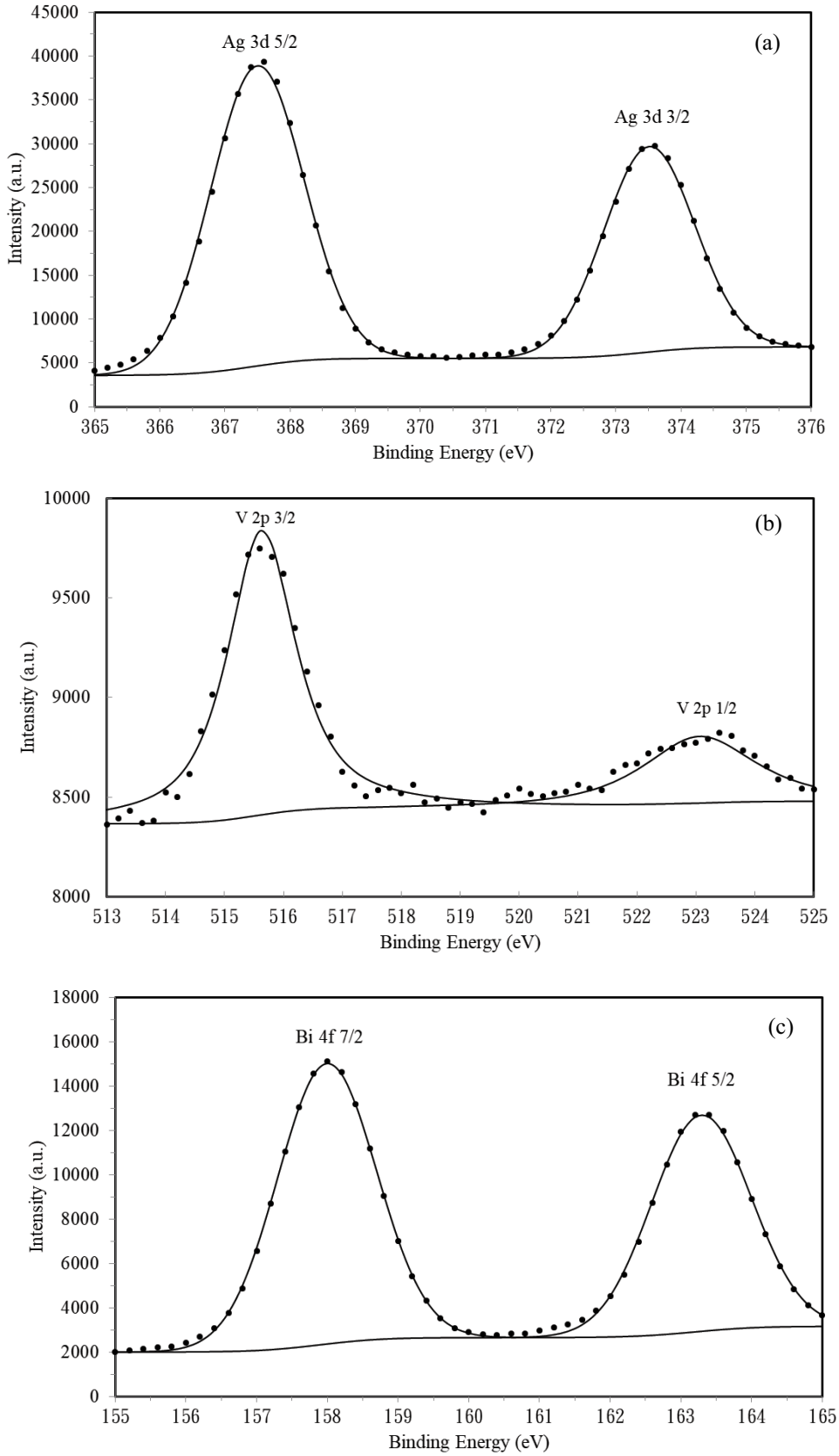

Fig. 5. Continued

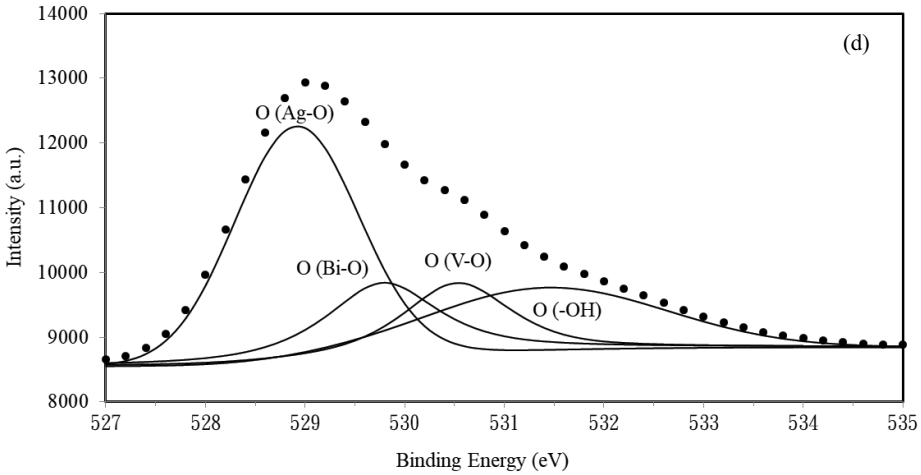

Fig. 5. XPS spectra of 1BAV (a) Ag_{3d}, (b) V_{2p}, (c) Bi_{4f}, and (d) O_{1s}.

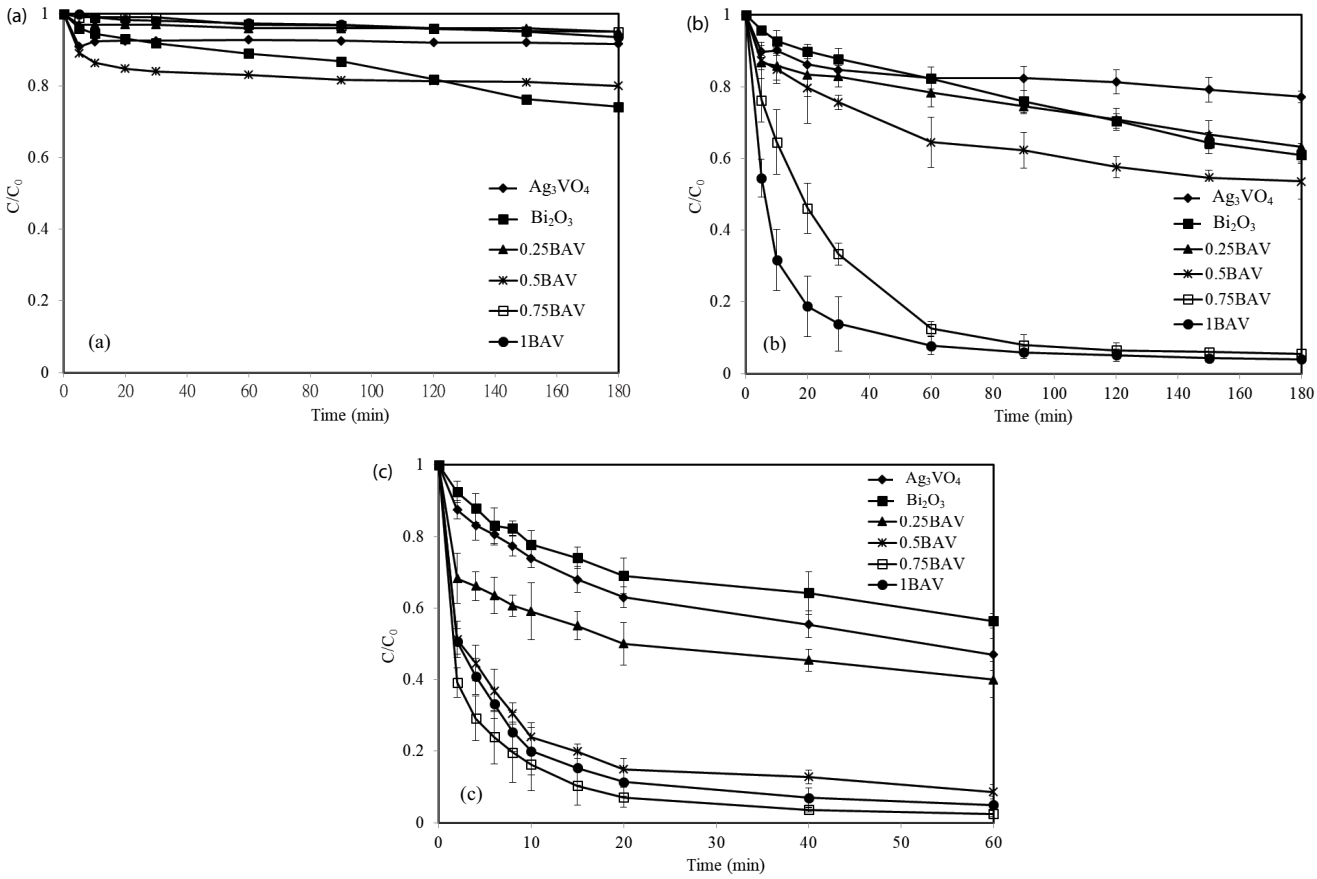

Fig. 6. Comparisons of RR2 removal by Ag_3VO_4, Bi_2O_3, and BAVs (a) adsorption, (b) Vis. Photocatalysis, and (c) UV photocatalysis ([RR2] = 20 mg/L, pH = 3, and [photocatalyst] = 0.5 g/L).

0.25BAV > Bi_2O_3 (Table 1). The *k* values of 0.75BAV and 1BAV in the photodegradation of RR2 were nearly 9 and 8 times that of pure Ag_3VO_4 under UV irradiation, respectively; approximately 34.4 and 65.9 times that of pure Ag_3VO_4 under Vis. irradiation, respectively, and about 7.9 and 23.8 times that of pure Ag_3VO_4 under solar irradiation, respectively (Table 1). These results demonstrate that the synergetic effect of the heterojunctions that form between Ag_3VO_4 and Bi_2O_3 is critical in increasing the photocatalytic activity of 0.75BAV and 1BAV, indicating the potential of 0.75BAV and 1BAV to photodegrade various organic pollutants in wastewaters under Vis. or solar irradiation. The BET

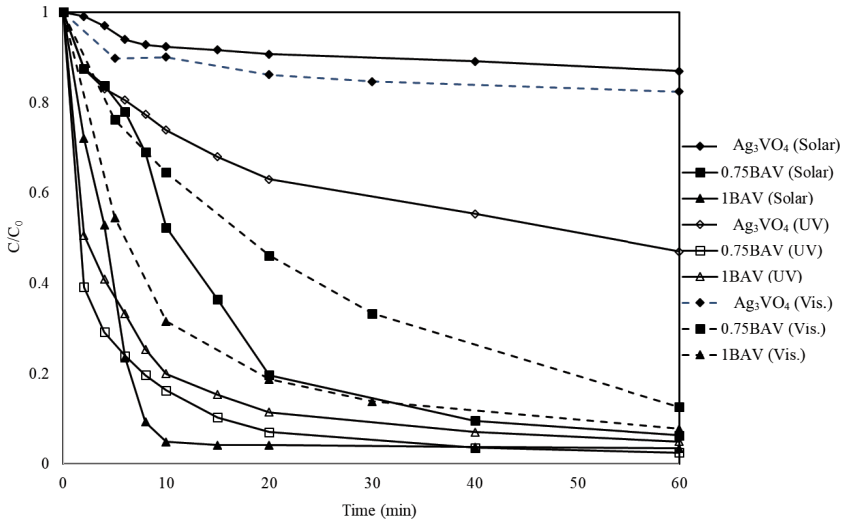

Fig. 7. Effects of light sources on RR2 photodegradation in the Ag_3VO_4, 0.75BAV, and 1BAV systems ([RR2] = 20 mg/L, pH = 3, and [photocatalyst] = 0.5 g/L).

surface area probably does not importantly influence the observed activity. The enhanced activity of the BAVs might be partially attributable to an increase in the efficiency of the separation of photo-generated electron-hole pairs in the BAVs, according to the PL study. Since the k values of 1BAV under Vis. and solar irradiation exceeded those of 0.75BAV, 1BAV was the best of the BAVs for photodegradation herein.

Reducing the Bi_2O_3 content reduces photocatalytic activity because it reduces heterojunction density. A higher Bi_2O_3 content provides lower photocatalytic activity because Bi_2O_3 particles cover active sites on the Ag_3VO_4 surface. Under Vis. or solar irradiation, 1BAV exhibited the highest photo-activity, whereas 0.75BAV exhibited the highest photo-activity under UV irradiation. This study found that the optimal Bi_2O_3 content on Ag_3VO_4 varied with the wavelength of the irradiating light on BAVs. As the amount of NiO loaded on Ag_3VO_4 increased, the reaction constant of Acid Red B photodegradation increased by a factor of 3.8 to Ag_3VO_4 at Ni 1.5 wt.%. The optimal amount of NiO trapped the highest number of photo-excited electrons, efficiently suppressing the recombination of photo-generated electron-holes, increasing the photocatalytic activity of NiO/Ag_3VO_4 [18]. Chen et al. [14] similarly found that the photocatalytic activity of $CaFe_2O_4$/Ag_3VO_4 increased with the amount of doped $CaFe_2O_4$ up to 2.0 wt.%. As the amount of doped $CaFe_2O_4$ increased above 2.0 wt.%, the photocatalytic activity of the samples declined. Xu et al. [10] found that the photocatalytic activity of La_2O_3/Ag_3VO_4 increases with La content up to 3 wt.%, and then decreases. When the amount of dopant exceeds the optimum value, the high concentration may provide recombination centers for the photo-generated electrons and holes, reducing the thickness of the space-charge layer on the surface of each photocatalyst particle, reducing the absorption of photons [14,18].

The stability of the photocatalysts importantly affects their practical application. The stability of 0.75BAV and 1BAV was evaluated by performing a cycling experiment (Fig. 8). After two cycling runs, the RR2 removal efficiency of 0.75BAV at 60 min declined from 84% to 83%, and that of 1BAV declined from 80% to 76%. The minor loss in photo-activity was attributed to photo-corrosion. After 60 min of the first-cycle reaction, the concentrations (percentages) of Ag that had leached from UV/Ag_3VO_4, UV/0.75BAV, and UV/1BAV systems were 391 (100%), 176 (86%), and 89 (50%) mg/L, respectively. Coupling Bi_2O_3 with Ag_3VO_4 significantly reduced the photo-corrosion of Ag from Ag_3VO_4.

Organic pollutants are well known to be decomposed by reactive species, such as superoxide anion radicals, photo-generated holes and hydroxyl radicals in photocatalytic reactions, which proceed irradiation. To examine potential photocatalytic mechanisms, active species trapping tests were performed during the degradation of RR2 by 1BAV, which yielded the results in Fig. 9. Introducing IPA, EDTA-2Na or Cr(VI) into the 1BAV system changed the RR2 photodegradation percentages by 0%, 64%, and 55%, respectively (Fig. 9). The fact that EDTA-2Na and Cr(VI) most strongly inhibited the photodegradation activity of 1BAV suggested that photo-generated holes and superoxide anion radicals were the dominant active species and that the photodegradation of RR2 in the 1BAV system was mainly governed by direct photo-generated hole and superoxide anion radical oxidation, as in the systems $ZnFe_2O_4$/Ag_3VO_4 [16], $ZnFe_2O_4$/Ag/Ag_3VO_4 [39], $CoFe_2O_4$/Ag/Ag_3VO_4 [40], g-C_3N_4/Ag_3VO_4 [5,6], BiOCl/Ag_3VO_4 [8], and Ag_3VO_4/Bi_2WO_6 [12,13].

The efficient separation of photo-generated electron-hole pairs is well known to be important in the photocatalytic activity of photocatalysts. The valence band (VB) and conduction band (CB) edge potentials of a semiconductor at the point of zero charge were calculated using Eqs. (2) and (3) [5,41,42]:

$$E_{CB} = X - E_e - 0.5\,E_g \quad (2)$$

$$E_{VB} = E_{CB} + E_g \quad (3)$$

where X is the absolute electronegativity of the semiconductors, given by the geometric mean of the absolute

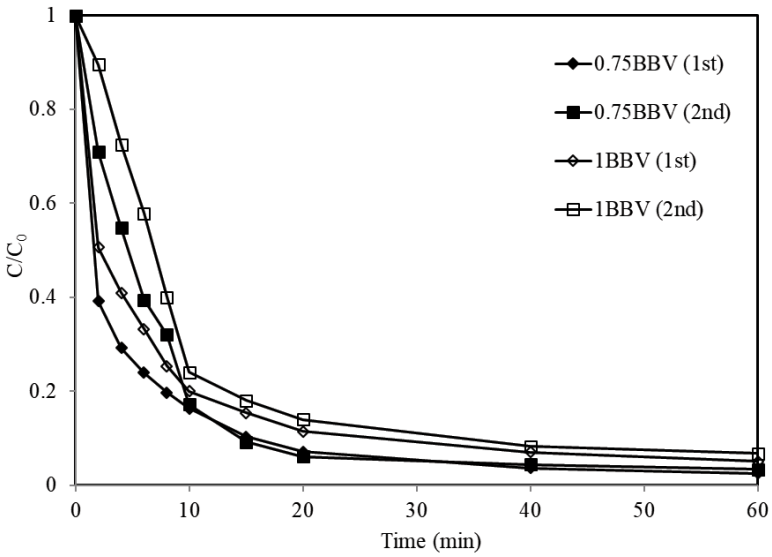

Fig. 8. Comparisons of cyclic photocatalysis of UV/0.75BAV and UV/1BAV systems ([RR2] = 20 mg/L, pH = 3, and [photocatalyst] = 0.5 g/L).

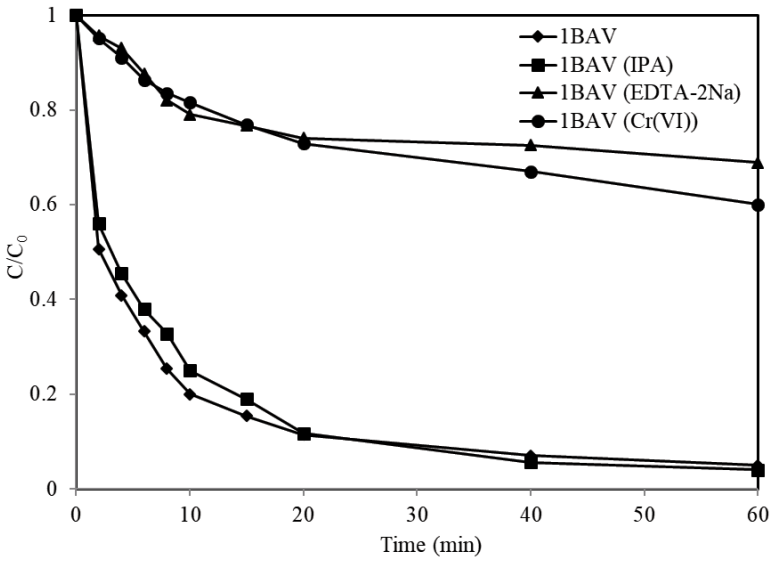

Fig. 9. Photocatalysis of RR2 by UV/1BAV in the presence of different scavengers ([RR2] = 20 mg/L, pH = 3, and [1BAV] = 0.5 g/L).

electronegativities of the constituent atoms. The absolute electronegativity is defined as the arithmetic mean of the atomic electron affinity and the first ionization energy. The X values of Bi_2O_3 and Ag_3VO_4 are 6.24 [43] and 5.65 eV [12,13,22], respectively. E_e is the energy of free electrons on the hydrogen scale (4.5 eV); E_g is the band gap of the photocatalyst, and E_{CB} and E_{VB} are the CB and VB edge potentials, respectively [42]. The E_g values for Bi_2O_3 and Ag_3VO_4 are 3.7 and 1.8 eV, respectively. The E_{CB} values for Bi_2O_3 and Ag_3VO_4 were calculated as 0.01 and 0.25 eV, respectively; the E_{VB} values were obtained as 3.71 and 2.05 eV, respectively. The above experimental calculations indicate that the CB of Ag_3VO_4 is more positive than that of Bi_2O_3 whereas the VB of Ag_3VO_4 is more negative than that of Bi_2O_3. Upon illumination of the BAVs by Vis., photo-generated electron-hole pairs are generated only on the Ag_3VO_4 moiety of the heterojunction, due to its narrow bandgap. The photo-generated electrons in the CB of Ag_3VO_4 are easily transferred to the VB of Bi_2O_3, because the CB energy of Ag_3VO_4 is more negative than the VB energy of Bi_2O_3. Accordingly, the charge carriers are effectively separated from each other and their recombination is substantially suppressed, increasing the lifetime of the photo-generated electron-hole pairs. Consequently, the photocatalytic activity of BAVs markedly exceeded those of pure Ag_3VO_4 and Bi_2O_3. Since the CB of Ag_3VO_4 (0.25 eV) is more positive than the potential of $O_2/{}^{\bullet}O^{2-}$ (–0.33 eV), the photo-generated electrons cannot reduce O_2–${}^{\bullet}O^{2-}$. However, the transformation of Ag^+ to Ag^0 frequently occurs in this

photocatalytic reaction system under irradiation. Ag^0 can be further excited to generated electrons, which may be trapped by adsorbed O_2 in water to form $^{\bullet}O^{2-}$ [13,21,40]. The increased number of photo-generated holes in the VB of Ag_3VO_4 cannot react with OH^- and H_2O to form $^{\bullet}OH$ because the potentials of the $^{\bullet}OH/OH^-$ (2.38 eV, vs. NHE) and $^{\bullet}OH/H_2O$ (2.72 eV, vs. NHE) exceed the VB of Ag_3VO_4 (2.05 eV, vs. NHE) (NHE – normal hydrogen electrode) [21]. Therefore, these photo-generated holes and superoxide anion radicals can directly degrade RR2 molecules by oxidation.

4. Conclusions

In this study, novel BAVs were successfully synthesized by the single-step hydrothermal method. The RR2 removal rate constants with Vis. photocatalysis followed the order 1BAV > 0.75BAV > 0.5BAV > Bi_2O_3 > 0.25BAV > Ag_3VO_4. The RR2 photodegradation rate constants of 0.75BAV and 1BAV were nearly 9 and 8 times that of pure Ag_3VO_4 under UV irradiation, respectively; approximately 34.4 and 65.9 times that of pure Ag_3VO_4 under Vis. irradiation, respectively; and about 7.8 and 23.8 times that of pure Ag_3VO_4 under solar irradiation, respectively. The results of this investigation suggest that the optimal Bi_2O_3 content in Ag_3VO_4 varied with the wavelength of irradiation on BAVs. The removal of RR2 in the 1BAV system is mainly governed by the direct oxidation of photo-generated holes and superoxide anion radicals. The combination of Ag_3VO_4 and Bi_2O_3 can increase the separation efficiency of photo-generated electron-hole pairs, reduce the photo-corrosion of Ag_3VO_4 and thereby enhance the photocatalytic activity of BAVs.

Acknowledgments

The authors would like to thank the Ministry of Science and Technology and National Kaohsiung University of Science and Technology, for financially supporting this research under Contract No. MOST 107-2221-E-992-001-MY2 and 109B01, respectively.

References

[1] R. Konta, H. Kato, H. Kobayashi, A. Kudo, Photophysical properties and photocatalytic activities under visible light irradiation of silver vanadates, Phys. Chem. Chem. Phys., 5 (2003) 3061–3065.
[2] L. Zhang, Y. He, P. Ye, Y. Wu, T. Wu, Enhanced photodegradation activity of Rhodamine B by $MgFe_2O_4/Ag_3VO_4$ under visible light irradiation, Catal. Commun., 30 (2013) 14–18.
[3] B. Inceesungvorn, T. Teeranunpong, J. Nunkaew, S. Suntalelat, D. Tantraviwat, Novel $NiTiO_3/Ag_3VO_4$ composite with enhanced photocatalytic performance under visible light, Catal. Commun., 54 (2014) 35–38.
[4] T. He, D. Wu, Y. Tan, Fabrication of $BiOI/BiVO_4$ heterojunction with efficient visible-light-induced photocatalytic activity, Mater. Lett., 165 (2016) 227–230.
[5] S. Wang, D. Li, C. Sun, S. Yang, Y. Guan, H. He, Synthesis and characterization of g-C_3N_4/Ag_3VO_4 composites with significantly enhanced visible-light photocatalytic activity for triphenylmethane dye degradation, Appl. Catal., B, 144 (2014) 885–892.
[6] S.Z. Wu, K. Li, W.D. Zhang, On the heterostructured photocatalysts Ag_3VO_4/g-C_3N_4 with enhanced visible light photocatalytic activity, Appl. Surf. Sci., 324 (2015) 324–331.
[7] T. Zhu, Y. Song, H. Ji, Y. Xu, Y. Song, J. Xia, S. Yin, Y. Li, H. Xu, Q. Zhang, H. Li, Synthesis of g-C_3N_4/Ag_3VO_4 composites with enhanced photocatalytic activity under visible light irradiation, Chem. Eng. J., 271 (2015) 96–105.
[8] P. Wang, H. Tang, Y. Ao, C. Wang, J. Hou, J. Qian, Y. Li, *In-situ* growth of Ag_3VO_4 nanoparticles onto BiOCl nanosheet to form a heterojunction photocatalyst with enhanced performance under visible light irradiation, J. Alloys Compd., 688 (2016) 1–7.
[9] X. Zou, Y. Dong, X. Zhang, Y. Cui, Synthesize and characterize of Ag_3VO_4/TiO_2 nanorods photocatalysts and its photocatalytic activity under visible light irradiation, Appl. Surf. Sci., 366 (2016) 173–180.
[10] H. Xu, H. Li, G. Sun, J. Xia, C. Wu, Z. Ye, Q. Zhang, Photocatalytic activity of La_2O_3-modified silver vanadates catalyst for Rhodamine B dye degradation under visible light irradiation, Chem. Eng. J., 160 (2010) 33–41.
[11] K. Wangkawong, S. Phanichphant, D. Tantraviwat, B. Inceesungvorn, $CoTiO_3/Ag_3VO_4$ composite: a study on the role of $CoTiO_3$ and the active species in the photocatalytic degradation of methylene blue, J. Colloid Interface Sci., 454 (2015) 210–215.
[12] S. Li, S. Hu, W. Jiang, Y. Liu, J. Liu, Z. Wang, Facile synthesis of flower-like Ag_3VO_4/Bi_2WO_6 heterojunction with enhanced visible-light photocatalytic activity, J. Colloid Interface Sci., 501 (2017) 156–163.
[13] J. Zhang, Z. Ma, Enhanced visible-light photocatalytic performance of Ag_3VO_4/Bi_2WO_6 heterojunctions in removing aqueous dyes and tetracycline hydrochloride, J. Taiwan Inst. Chem. Eng., 78 (2017) 212–218.
[14] S. Chen, W. Zhao, W. Liu, H. Zhang, X. Yu, Y. Chen, Preparation, characterization and activity evaluation of p–n junction photocatalyst p-$CaFe_2O_4$/n-Ag_3VO_4 under visible light irradiation, J. Hazard. Mater., 172 (2009) 1415–1423.
[15] L. Zhang, Y. He, P. Ye, W. Qin, Y. Wu, T. Wu, Enhanced photodegradation activity of Rhodamine B by Co_3O_4/Ag_3VO_4 under visible light irradiation, Mater. Sci. Eng., B, 178 (2013) 45–52.
[16] L. Zhang, Y. He, P. Ye, Y. Wu, T. Wu, Visible light photocatalytic activities of $ZnFe_2O_4$ loaded by Ag_3VO_4 heterojunction composites, J. Alloys Compd., 549 (2013) 105–113.
[17] S. Wang, Y. Guan, L. Wang, W. Zhao, H. He, J. Xiao, S. Yang, C. Sun, Fabrication of a novel bifunctional material of BiOI/Ag_3VO_4 with high adsorption-photocatalysis for efficient treatment of dye wastewater, Appl. Catal., B, 168–169 (2015) 448–457.
[18] X. Hu, C. Hu, Preparation and visible-light photocatalytic activity of Ag_3VO_4 powders, J. Solid State Chem., 180 (2007) 725–732.
[19] V.R. Raja, D.R. Rosaline, A. Suganthi, M. Rajarajan, Ultrasonic assisted synthesis with enhanced visible-light photocatalytic activity of NiO/Ag_3VO_4 nanocomposite and its antibacterial activity, Ultrason. Sonochem., 44 (2018) 73–85.
[20] T. Zhang, M. Liu, Y. Meng, B. Huang, X. Pu, X. Shao, A novel method for the synthesis of $Ag_3VO_4/Ag_2VO_2PO_4$ heterojunction photocatalysts with improved visible-light photocatalytic properties, Sep. Purif. Technol., 206 (2018) 149–157.
[21] J. Zhang, Z. Ma, $Ag_3VO_4/BiOIO_3$ heterojunction with enhanced visible-light-driven catalytic activity, J. Taiwan Inst. Chem. Eng., 88 (2018) 177–185.
[22] J. Zhang, Z. Ma, Flower-like Ag_3VO_4/BiOBr n-p heterojunction photocatalysts with enhanced visible-light-driven catalytic activity, Mol. Catal., 436 (2017) 190–198.
[23] M. Su, C. He, V.K. Sharma, M.A. Asi, D. Xia, X.Z. Li, H. Deng, Y. Xiong, Mesoporous zinc ferrite: synthesis, characterization, and photocatalytic activity with H_2O_2/visible light, J. Hazard. Mater., 211–212 (2012) 95–103.
[24] T. Li, S. Luo, Hydrothermal synthesis of Ag_2O/Bi_2O_3 microspheres for efficient photocatalytic degradation of Rhodamine B under visible light irradiation, Ceram. Int., 41 (2015) 13135–13146.
[25] H. Yuan, J. Liu, J. Li, Y. Li, X. Wang, Y. Zhang, J. Jiang, S. Chen, C. Zhao, D. Qian, Designed synthesis of a novel $BiVO_4$–Cu_2O–TiO_2 as an efficient visible-light-resonding photocatalyst, J. Colloid Interface Sci., 444 (2015) 58–66.
[26] L. Yue, S. Wang, G. Shan, W. Wu, L. Qiang, L. Zhu, Novel MWNTs-Bi_2WO_6 composites with enhanced simulated solar

photoactivity toward adsorbed and free tetracycline in water, Appl. Catal., B, 176–177 (2015) 11–19.
[27] L. Zhang, H. Wang, Z. Chen, P.K. Wong, J. Liu, Bi_2WO_6 micro/nano-structures: synthesis, modifications and visible-light-driven photocatalytic applications, Appl. Catal., B, 106 (2011) 1–13.
[28] Z. Zhang, W. Wang, D. Jiang, J. Xu, Synthesis of dumbbell-like Bi_2WO_6@$CaWO_4$ composite photocatalyst and application in water treatment, Appl. Surf. Sci., 292 (2014) 948–953.
[29] L.Q. Jing, Y.C. Qu, B.Q. Wang, S.D. Li, B.J. Jiang, L.B. Yang, W. Fu, H.G. Fu, J.Z. Sun, Review of photoluminescence performance of nano-sized semiconductor materials and its relationships with photocatalytic activity, Sol. Energy Mater. Sol. Cells, 90 (2006) 1773–1787.
[30] M. Shang, W. Wang, L. Zhang, H. Xu, Bi_2WO_6 with significantly enhanced photocatalytic activities by nitrogen doping, Mater. Chem. Phys., 120 (2010) 155–159.
[31] H. Li, Y. Cui, W. Hong, High photocatalytic performance of BiOI/Bi_2WO_6 toward toluene and reactive brilliant red, Appl. Surf. Sci., 264 (2013) 581–588.
[32] X.Y. Li, X.J. Zou, Z.P. Qu, Q.D. Zhao, L.Z. Wang, Photocatalytic degradation of gaseous toluene over Ag-doping TiO_2 nanotube powder prepared by anodization coupled with impregnation method, Chemosphere, 83 (2011) 674–679.
[33] L. Schacht, J. Navarrete, P. Schacht, M.A. Ramirez, Influence of vanadium oxidation states on the performance of V–Mg–Al mixed-oxide catalysts for the oxidative dehydrogenation of propane, J. Mex. Chem. Soc., 54 (2010) 69–73.
[34] Y. Xie, Y. Dai, X. Yuan, L. Jiang, L. Zhou, Z. Wu, J. Zhang, H. Wang, T. Xiong, Insight on the plasmonic Z-scheme mechanism underlying the highly efficient photocatalytic activity of silver molybdate/silver vanadate composite in rhodamine B degradation, J. Colloid Interface Sci., 530 (2018) 493–504.
[35] X. Du, J. Wan, J. Jia, C. Pan, X. Hu, J. Fan, E. Liu, Photocatalystic degradation of RhB over highly visible-light-active Ag_3PO_4-Bi_2MoO_6 heterojunction using H_2O_2 electron capturer, Mater. Des., 119 (2017) 113–123.
[36] X. Ding, K. Zhao, L. Zhang, Enhanced photocatalytic removal of sodium pentachlorophenate with self-doped Bi_2WO_6 under visible light by generating more superoxide ions, Environ. Sci. Technol., 48 (2014) 5823–5831.
[37] J. Sun, X. Li, Q. Zhao, M.O. Tadé, S. Liu, Construction of p-n heterojunction β-Bi_2O_3/$BiVO_4$ nanocomposite with improved photoinduced charge transfer property and enhanced activity in degradation of ortho-dichlorobenzene, Appl. Catal., B, 219 (2017) 259–268.
[38] R. Ran, X. Meng, Z. Zhang, Facile preparation of novel graphene oxide-modified Ag_2O/Ag_3VO_4/$AgVO_3$ composites with high photocatalytic activities under visible light irradiation, Appl. Catal., B, 196 (2016) 1–15.
[39] L. Jing, Y. Xu, C. Qin, J. Liu, S. Huang, M. He, H. Xu, H. Li, Visible-light-driven $ZnFe_2O_4$/Ag/Ag_3VO_4 photocatalysts with enhanced photocatalytic activity under visible light irradiation, Mater. Res. Bull., 95 (2017) 607–615.
[40] L. Jing, Y. Xu, S. Huang, M. Xie, M. He, H. Xu, H. Li, Q. Zhang, Novel magnetic $CoFe_2O_4$/Ag/Ag_3VO_4 composites: highly efficient visible light photocatalytic and antibacterial activity, Appl. Catal., B, 199 (2016) 11–22.
[41] X. Meng, Z. Zhang, Bismuth-based photocatalytic semiconductors: introduction, challenges and possible approaches, J. Mol. Catal. A: Chem., 423 (2016) 533–549.
[42] Q. Shi, W. Zhao, L. Xie, J. Chen, M. Zhang, Y. Li, Enhanced visible-light driven photocatalytic mineralization of indoor toluene via a $BiVO_4$/reduced graphene oxide/Bi_2O_3 all-solid-state Z-scheme system, J. Alloys Compd., 662 (2016) 108–117.
[43] Y. Wang, Y. He, T. Li, J. Cai, M. Luo, L. Zhao, Photocatalytic degradation of methylene blue on $CaBi_6O_{10}$/Bi_2O_3 composites under visible light, Chem. Eng. J., 189–190 (2012) 473–481.